ISSN (Print) 1226-1750
ISSN (Online) 2233-6656
Journal of Magnetics 25(2), 117-120 (2020) https://doi.org/10.4283/JMAG.2020.25.2.117

Crystallographic and Magnetic Characteristics of Thin-film $Ni_{0.5}Co_{0.5}Fe_2O_4$ Ferrimagnet

Kwang Joo Kim[1], Jongho Park[1], and Jae Yun Park[2]*

[1]*Department of Physics, Konkuk University, Seoul 05029, Republic of Korea*
[2]*Department of Materials Science and Engineering, Incheon National University, Incheon 22012, Republic of Korea*

(Received 28 February 2020, Received in final form 22 April 2020, Accepted 27 April 2020)

Crystallographic and magnetic characteristics of thin-film $Ni_{0.5}Co_{0.5}Fe_2O_4$ ferrimagnet prepared by a sol-gel deposition method were investigated by X-ray diffraction, Raman spectroscopy, X-ray photoelectron spectroscopy (XPS), and vibrating sample magnetometry (VSM). The mixed ferrite $Ni_{0.5}Co_{0.5}Fe_2O_4$ specimen was found to be polycrystalline having cubic spinel structure with slightly reduced lattice constant compared to $CoFe_2O_4$. The XPS data indicate that Co and Ni ions in $Ni_{0.5}Co_{0.5}Fe_2O_4$ have charge valence of +2. The VSM measurements indicate that the $Ni_{0.5}Co_{0.5}Fe_2O_4$ film have saturation magnetization, remanent magnetization, and coercivity of 257 emu/cm^3, 115 emu/cm^3, and 0.5 kOe, respectively, which are 62 %, 68 %, and 29 % of those of $CoFe_2O_4$. The reduction of the magnetic parameters of $Ni_{0.5}Co_{0.5}Fe_2O_4$ compared to $CoFe_2O_4$ is primarily attributable to the smaller magnetic moment of high-spin Ni^{2+} ion (2 μ_B) than that of Co^{2+} ion (3 μ_B).

Keywords : crystallographic, ferrite, thin film, magnetic properties

1. Introduction

Cobalt ferrite ($CoFe_2O_4$) is one of the spinel compounds in which the magnetic ions occupy either 8*a* (tetrahedral) or 16*d* (octahedral) sites surrounded by four and six oxygen anions (O^{2-}), respectively, at the 32*e* sites. The magnetic properties of $CoFe_2O_4$ tend to be significantly affected by the location of Co^{2+} ion in either tetrahedral (A) or octahedral (B) sites. When $CoFe_2O_4$ is in pristine inverse-spinel state, A sites are occupied by only Fe^{3+} ions with the magnetic moment of 5 μ_B, while B sites are occupied by Fe^{3+} and Co^{2+} ions with 5 μ_B and 3 μ_B, respectively. The anti-parallel alignment of magnetic moment between A and B sites results in ferrimagnetism with the net magnetic moment of 3 μ_B per formula unit, equivalent to 380 emu/cm^3 (= 76 emu/g).

In reality, experimental evidences have suggested that some of the Co^{2+} ions in $CoFe_2O_4$ occupy A sites [1-3]. The degree of inversion δ [4] for the ionic configuration $(Co^{2+}_{1-\delta}Fe^{3+}_{\delta})^A[Co^{2+}_{\delta}Fe^{3+}_{2-\delta}]^BO_4$ is likely to be dependent on the synthetic methods of the ferrimagnet [1, 2, 5, 6] and affects its physical properties, e.g., crystallographic, electrical, and magnetic characteristics. As a ferrimagnetic insulator, $CoFe_2O_4$ has been drawing research interest for a wide range of applications including refrigeration, microwave sensing, and biomedicine. With such a variety of potentials, new ferrimagnetic oxides derivable from $CoFe_2O_4$ are worthwhile to be studied. For example, the magnetic properties of the ferrimagnet are variable by replacing Co^{2+} ions without changing the crystal structure.

The objective of the present study is to investigate the crystallographic and magnetic properties and the related electronic structure of $Ni_{0.5}Co_{0.5}Fe_2O_4$ focusing on the physical changes as Co^{2+} ions are replaced by Ni^{2+} ions in the spinel lattice ($CoFe_2O_4 \rightarrow Ni_{0.5}Co_{0.5}Fe_2O_4$). The crystallographic properties of the present sol-gel prepared $Ni_{0.5}Co_{0.5}Fe_2O_4$ thin film were investigated by X-ray diffraction (XRD) and Raman spectroscopy. The electronic structure of $Ni_{0.5}Co_{0.5}Fe_2O_4$ including ionic valences of Ni, Co, and Fe were investigated by X-ray photoelectron spectroscopy (XPS). The magnetic hysteresis curve of the $Ni_{0.5}Co_{0.5}Fe_2O_4$ specimen was investigated by vibrating sample magnetometry (VSM).

2. Experimental

The $Ni_{0.5}Co_{0.5}Fe_2O_4$ samples were provided by using a sol-gel deposition method on Si(100) substrates under the

*Corresponding author: Tel: +82-32-835-8271
Fax: +82-32-835-0778, e-mail: pjy@inu.ac.kr

following sequence. (1) Preparation of the precursor solution by dissolving $Fe(NO_3)_3{\cdot}9H_2O$, $Co(CH_3CO_2)_2{\cdot}4H_2O$, and $Ni(CH_3CO_2)_2{\cdot}4H_2O$ in 2-methoxyethanol (20 ml) and ethanolamine (2 ml) at 110 °C. (2) Repetition of spin-coating the substrate using the precursor solution at 3000 rpm for 20 s followed by pre-heating at 300 °C for 5 min. (3) Post-annealing of the gel film in air at 800 °C for 4 h.

The crystalline structure of the specimen was monitored by using XRD (Cu K_α line, wavelength = 0.15418 nm) in the grazing-incidence geometry with fixed X-ray incidence angle of 4°. The vibrational modes of the specimen were investigated by Raman scattering spectroscopy employing a diode laser (wavelength = 514 nm, power = 1 mW). The XPS measurements on the specimen were performed using Al K_α line (photon energy = 1486.7 eV). The magnetic hysteresis curve of the specimen was measured by using VSM at room temperature. The magnetic field was applied parallel to the film's plane up to 15 kOe.

3. Results and Discussion

The present $Ni_{0.5}Co_{0.5}Fe_2O_4$ thin-film specimen had phase purity with no secondary phase as shown in the XRD pattern in Fig. 1. The XRD pattern of the $Ni_{0.5}Co_{0.5}Fe_2O_4$ specimen is compared with that of a $CoFe_2O_4$ specimen prepared under the same sol-gel process [7]. The estimated lattice constant of the $Ni_{0.5}Co_{0.5}Fe_2O_4$ specimen is 0.8350 nm, slightly smaller than that of the $CoFe_2O_4$ film (0.8358 nm).

In Figs. 2(a) and 2(b), representative top- and side-view images, respectively, of the $Ni_{0.5}Co_{0.5}Fe_2O_4$ specimen observed by scanning electron microscopy (SEM) are exhibited. The SEM images revealed typical microstructures containing well-defined $Ni_{0.5}Co_{0.5}Fe_2O_4$ grains with various sizes (50-200 nm). The side-view image shows quite a flat and smooth surface of the film with the thickness near 375 nm.

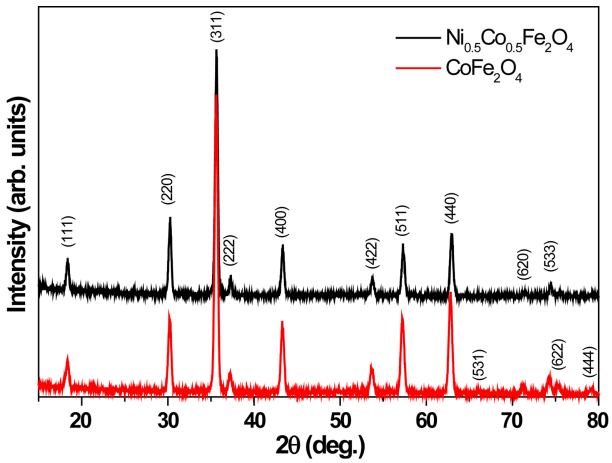

Fig. 1. (Color online) X-ray diffraction pattern of thin-film $Ni_{0.5}Co_{0.5}Fe_2O_4$ compared to $CoFe_2O_4$.

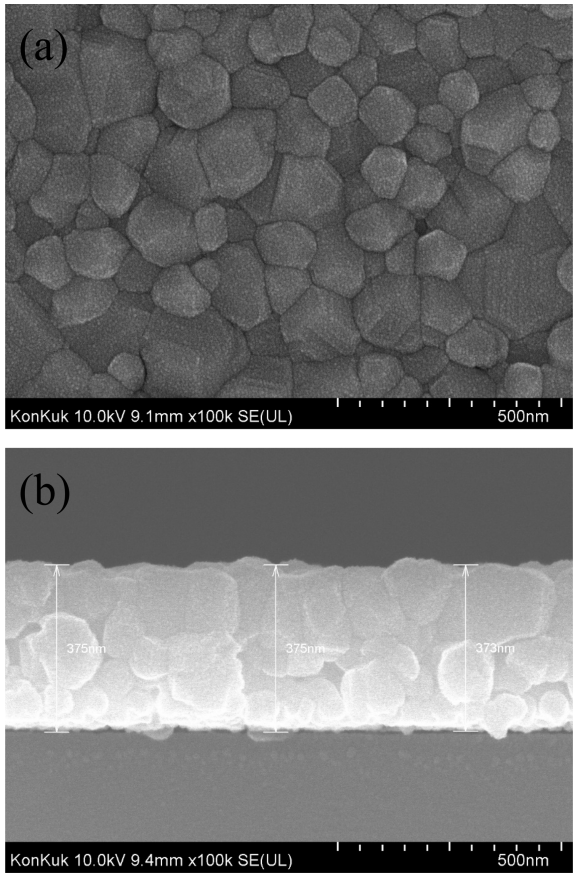

Fig. 2. Typical scanning electron microscopy images of sol-gel-deposited $Ni_{0.5}Co_{0.5}Fe_2O_4$ film: (a) top view and (b) side view.

In Fig. 3(a), Ni 2*p*-electron binding-energy (B-E) spectrum of the $Ni_{0.5}Co_{0.5}Fe_2O_4$ specimen obtained by using XPS is exhibited. The two major peaks at 854 and 872 eV are ascribed to the spin-orbit splitting, $2p_{3/2}$ and $2p_{1/2}$, respectively, of Ni 2*p* states. The energy difference of 18 eV between the two peaks suggests a +2 oxidation state of the Ni ion [8]. In Fig. 3(b), Co 2*p*-electron B-E spectrum of the $Ni_{0.5}Co_{0.5}Fe_2O_4$ specimen exhibits the $2p_{3/2}$ and $2p_{1/2}$ peaks at 780 and 795 eV, respectively. The observed $2p_{3/2}$–$2p_{1/2}$ splitting of 15 eV suggests a +2 oxidation state of the Co ion [9]. Such single valence of both Co and Ni ions suggests that the Fe ions in $Ni_{0.5}Co_{0.5}Fe_2O_4$ have a +3 oxidation state mostly. For both the Ni and Co 2*p* spectra, both the $2p_{3/2}$ and $2p_{1/2}$ peaks entail intensive satellite peaks at the higher B-E. These satellites are mainly attributable to the energy loss of the photoelectrons due to their interaction with the magnetic cations.

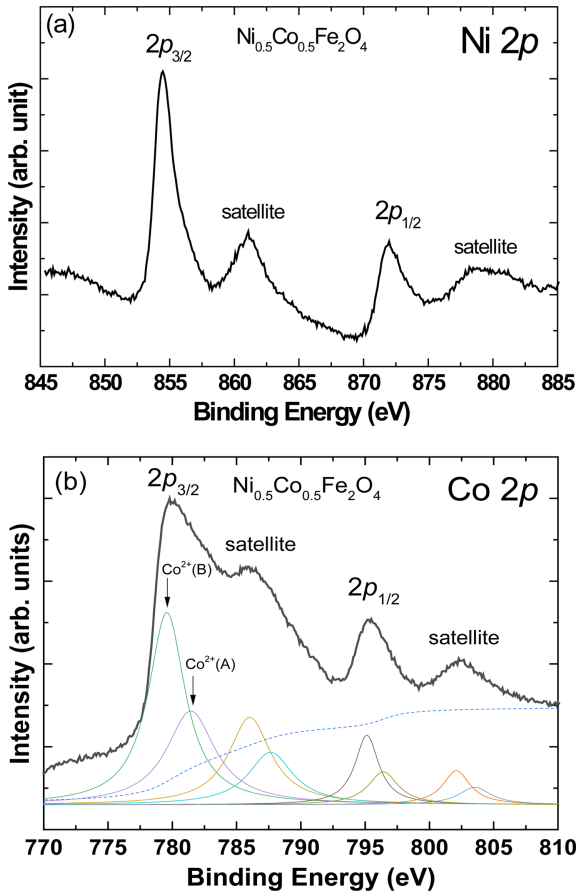

Fig. 3. (Color online) X-ray photoelectron spectra of (a) Ni 2*p* and (b) Co 2*p* electrons of $Ni_{0.5}Co_{0.5}Fe_2O_4$ film. Solid curves below the experimental spectrum represent result of curve-fitting. Dashed line below the experimental spectrum represents background.

The asymmetric shapes of the Co $2p_{3/2}$ and $2p_{1/2}$ peaks in Fig. 3(b) compared to those of the Ni 2*p* spectrum in Fig. 3(a) suggest that the photoelectron peaks are composed of two origins, Co^{2+}(B) and Co^{2+}(A) at the higher B-E. So, each peak in the Co 2*p* spectrum can be fitted by two sub-peaks as shown in Fig. 3(b). The B-E difference between the two sub-peaks for $2p_{3/2}$ is estimated to be 2.0 eV.

In Fig. 4, the Raman spectrum of the $Ni_{0.5}Co_{0.5}Fe_2O_4$ specimen is exhibited in comparison with that of $CoFe_2O_4$ [7]. The Raman peaks above 600 cm^{-1} are ascribed to A_{1g} vibrational modes for symmetric stretching of O^{2-} ions at the A sites [10, 11]. Consequently, the peaks at 693 and 615 cm^{-1} for $CoFe_2O_4$ are assigned to $A_{1g}(Fe^{3+}\text{-}O^{2-})$ and $A_{1g}(Co^{2+}\text{-}O^{2-})$, respectively [11]. The peaks below 600 cm^{-1} for $CoFe_2O_4$ are assigned to T_{2g} (580, 470, 207 cm^{-1}) and E_g (305 cm^{-1}) vibrational modes corresponding to symmetric and anti-symmetric bending of O^{2-} ions at the B sites, respectively [11, 12]. Especially, the peak at 470

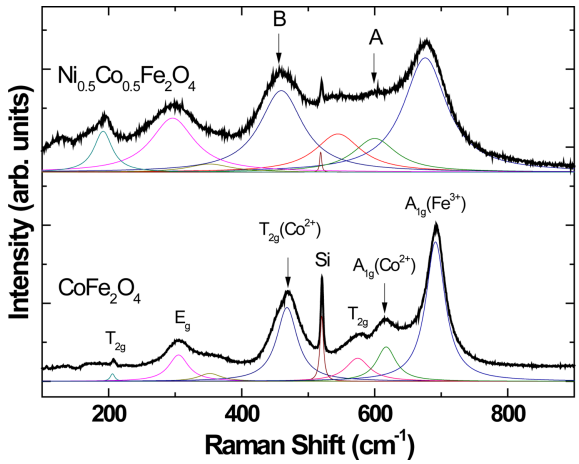

Fig. 4. (Color online) Raman shifts of thin-film $Ni_{0.5}Co_{0.5}Fe_2O_4$ compared to $CoFe_2O_4$. Solid curves below the experimental spectra represent result of curve-fitting.

cm^{-1}, absent in the Raman spectra of Fe_3O_4 [13], is strong for $CoFe_2O_4$ [11, 12]. It is assigned to T_{2g} mode involving Co^{2+}(B) ions. Thus, the Raman spectrum of $CoFe_2O_4$ exhibits peaks for tetrahedral (615 cm^{-1}) and octahedral (470 cm^{-1}) Co^{2+} ions together [11, 14].

The Raman spectrum for the $Ni_{0.5}Co_{0.5}Fe_2O_4$ specimen exhibits a similar pattern to that of $CoFe_2O_4$: the peaks of the former are broadened and shifted to the lower energies compared to those of the latter, e.g., the $A_{1g}(Fe^{3+})$ peak is located at 678 cm^{-1} and the $T_{2g}(Co^{2+})$ peak is located at 460 cm^{-1} for $Ni_{0.5}Co_{0.5}Fe_2O_4$.

The intensity of each Raman peak could be evaluated by a curve-fitting as shown in Fig. 4. Among the fitted curves, the ratio of the curve areas of $A_{1g}(Co^{2+})$ and $T_{2g}(Co^{2+})$ peaks, marked by A and B, respectively, could be interpreted as the ratio of Co^{2+}(A) and Co^{2+}(B) ions in the compound. The estimated ratio N(A):N(B) is 29:71 for $Ni_{0.5}Co_{0.5}Fe_2O_4$ and 30:70 for $CoFe_2O_4$. Thus, the two specimens have the ratio of Co^{2+}(A)/Co^{2+}(B) close to each other. Considering the tendency of octahedral preference of Ni^{2+} ions in spinel oxides [15, 16], the $Ni_{0.5}Co_{0.5}Fe_2O_4$ specimen is expected to have the ionic distribution of $(Co^{2+}_{0.15}Fe^{3+}_{0.85})^{A}[Co^{2+}_{0.35}Ni^{2+}_{0.50}\ Fe^{3+}_{1.15}\ ]^{B}O_4$.

The magnetic hysteresis curve of the $Ni_{0.5}Co_{0.5}Fe_2O_4$ specimen is exhibited in comparison with that of $CoFe_2O_4$ [7] in Fig. 5. The result indicates that the $Ni_{0.5}Co_{0.5}Fe_2O_4$ film have saturation magnetization (M_s), remanent magnetization (M_r), and coercivity (H_c) of 257 emu/cm^3, 115 emu/cm^3, and 0.5 kOe, respectively. These values are smaller than those of $CoFe_2O_4$: 415 emu/cm^3 (M_s), 170 emu/cm^3 (M_r), and 1.7 kOe (H_c) [7]. The magnetic parameters of $Ni_{0.5}Co_{0.5}Fe_2O_4$ are reduced to 62 % (M_s), 68 % (M_r), and 29 % (H_c) of those of $CoFe_2O_4$.

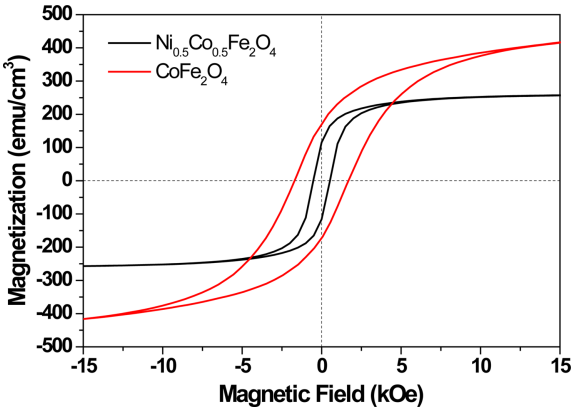

Fig. 5. (Color online) Magnetic hysteresis curve of thin-film $Ni_{0.5}Co_{0.5}Fe_2O_4$ compared to $CoFe_2O_4$.

The reduction of the saturation magnetization of $Ni_{0.5}Co_{0.5}Fe_2O_4$ compared to that of $CoFe_2O_4$ can be explained by taking the magnetic moment of high-spin Ni^{2+}, Co^{2+}, and Fe^{3+} as 2, 3, and 5 μ_B, respectively. Then, the net magnetic moment of $Ni_{0.5}Co_{0.5}Fe_2O_4$ with the ionic distribution of $(Co^{2+}_{0.15}Fe^{3+}_{0.85})^A[Co^{2+}_{0.35}Ni^{2+}_{0.50}Fe^{3+}_{1.15}]^BO_4$ is evaluated to be 3.1 μ_B per formula unit. For $CoFe_2O_4$ with $(Co^{2+}_{0.3}Fe^{3+}_{0.7})^A[Co^{2+}_{0.7}Fe^{3+}_{1.3}]^BO_4$, the net magnetic moment becomes 4.2 μ_B. This theoretical estimation predicts that the value of M_s for $Ni_{0.5}Co_{0.5}Fe_2O_4$ is reduced to 74 % of that of $CoFe_2O_4$. Thus, the decrease of M_s for $Ni_{0.5}Co_{0.5}Fe_2O_4$ compared to $CoFe_2O_4$ is primarily ascribed to the decrease of magnetic moment per ferrimagnetic formula unit of the compound through the replacement of Co^{2+} (3 μ_B) by Ni^{2+} (2 μ_B).

4. Conclusions

Thin-film $Ni_{0.5}Co_{0.5}Fe_2O_4$ prepared by the present sol-gel process exhibits spinel structure with the lattice parameter slightly smaller (by 0.1 %) than that of $CoFe_2O_4$. The XPS result indicates that both Ni and Co ions have charge valence of +2. The XPS analysis also suggests that the Co ions occupy the tetrahedral as well as the octahedral sites, while the Ni ions occupy mostly the octahedral sites of the spinel lattice. The Raman spectroscopy analysis implies that ~30 % of Co^{2+} ions occupy the tetrahedral sites for both the cobalt-ferrimagnets. The VSM measurement indicates that M_s, M_r, and H_c of $Ni_{0.5}Co_{0.5}Fe_2O_4$ are reduced to 62 %, 68 %, and 29 %, respectively, of those of $CoFe_2O_4$. The reduction of the magnetic parameters by the Ni switching is primarily ascribed to the smaller magnetic moment of high-spin Ni^{2+} ion than that of Co^{2+} ion.

Acknowledgment

This work was supported by Incheon National University Research Grant in 2018.

References

[1] S. S. Bellad and C. H. Bhosale, Thin Solid Films **322**, 93 (1998).
[2] Y. Li, Q. Fang, Y. Liu, Q. Lv, and P. Yin, J. Magn. Magn. Mater. **313**, 57 (2007).
[3] Z. Zhou, Y. Zhang, Z. Wang, W. Wei, W. Tang, J. Shi, and R. Xiong, Appl. Surf. Sci. **254**, 6972 (2008).
[4] R. N. Bhowmik, A. T. Satya, and A. Bharathi, J. Alloys Comp. **559**, 134 (2013).
[5] P. D. Thang, G. Rijnders, and D. H. A. Blank, J. Magn. Magn. Mater. **310**, 2621 (2007).
[6] W. Fu, S. Liu, W. Fan, H. Yang, X. Pang, J. Xu, and G. Zou, J. Magn. Magn. Mater. **316**, 54 (2007).
[7] K. J. Kim and J. Park, J. Sol-Gel Sci. Technol. **92**, 40 (2019).
[8] J. H. Lee and K. J. Kim, Electrochim. Acta **137**, 169 (2014).
[9] R. S. Yadav, I. Kuřitka, J. Vilcakova, J. Havlica, J. Masilko, L. Kalina, J. Tkacz, J. Švec, V. Enev, and M. Hajdúchová, Adv. Nat. Sci.: Nanosci. Nanotechnol. **8**, 045002 (2017).
[10] Z. Wang, R. T. Downs, V. Pischedda, R. Shetty, S. K. Saxena, C. S. Zha, Y. S. Zhao, D. Schiferl, and A. Waskowska, Phys. Rev. B **68**, 094101 (2003).
[11] V. Georgiadou, V. Tangoulis, I. Arvanitidis, O. Kalogirou, and C. Dendrinou-Samara, J. Phys. Chem. C **119**, 8336 (2015).
[12] P. Chandramohan, M. P. Srinivasan, S. Velmurugan, and S. V. Narasimhan, J. Solid State Chem. **184**, 89 (2011).
[13] S. Tiwari, R. J. Choudhary, R. Prakash, and D. M. Phase, J. Phys.: Condens. Matter. **19**, 176002 (2007).
[14] D. Sharma and N. Khare, Appl. Phys. Lett. **105**, 032404 (2014).
[15] P. P. Hankare, K. R. Sanadi, K. M. Garadkar, D. R. Patil, and I. S. Mulla, J. Alloys Comp. **553**, 383 (2013).
[16] A. K. Singh, T. C. Goel, and R. G. Mendiratta, Solid State Commun. **125**, 121 (2003).